

***Smad4* controls proliferation of interstitial cells in the neonatal kidney**

Sarah S. McCarthy¹, Michele Karolak¹, and Leif Oxburgh^{2,*}

¹Maine Medical Center Research Institute, Scarborough ME, 04074, USA

²The Rogosin Institute, New York, NY, 10065, USA

Keywords: Smad, TGF β , Wnt

*Author for correspondence: Email: leo9022@nyp.org. Mailing address: The Rogosin Institute, 310 East 67th Street, New York, NY 10065.

Summary statement: This study describes a novel function for TGF β signaling in the developing renal interstitium. Mice with *Foxd1*cre-mediated deletion of *Smad4* have interstitial expansion and activated Wnt signaling.

ABSTRACT

Expansion of interstitial cells in the adult kidney is a hallmark of chronic disease, whereas their proliferation during fetal development is necessary for organ formation. An intriguing difference between adult and neonatal kidneys is that the neonatal kidney has the capacity to control interstitial cell proliferation when the target number has been reached. In this study, we define the consequences of inactivating the TGF β /Smad response in the interstitial cell lineage. We find that pathway inactivation through loss of *Smad4* leads to over-proliferation of interstitial cells regionally in the kidney medulla. Analysis of markers for BMP and TGF β pathway activation reveals that loss of *Smad4* primarily reduces TGF β signaling in the interstitium. While TGF β signaling is reduced in these cells, marker analysis shows that Wnt/ β -catenin signaling is increased. Our analysis supports a model in which Wnt/ β -catenin mediated proliferation is attenuated by TGF β /Smad to ensure that proliferation ceases when the target number of interstitial cells has been reached in the neonatal medulla.

INTRODUCTION

Interstitial cells are any cells located between the functional cells, or parenchyma, of a tissue. In the kidney, cells of the nephron and blood vessel are considered the functional components and the interstitial cell population is made up largely of PDGFR β -expressing fibroblasts. These cells derive from the *Foxd1* expressing progenitor, which also gives rise to mesangial cells, the specialized pericytes of the glomerulus. Expansion of interstitial cells in the adult kidney is a hallmark of chronic disease, with unopposed interstitial cell proliferation leading to progressive scarring (fibrosis) and concomitant loss of parenchyma (Humphreys et al., 2010). In contrast, proliferation of interstitial cells plays an essential role in fetal development and somatic growth of the kidney (Boivin and Bridgewater, 2018; Das et al., 2013; Fetting et al., 2014; Hatini et al., 1996). An intriguing difference between adult and neonatal kidneys is that the neonatal kidney has the capacity to control interstitial cell proliferation when the target number has been reached, and our study aims to characterize basic mechanisms of this proliferation control.

Gene inactivation and experimental therapeutics targeting the TGF β signaling pathway have been used to reduce fibrosis in kidney injury models (Inazaki et al., 2004; Morishita et al., 2014), indicating that the pathway is a significant driver of interstitial expansion. We therefore hypothesized that the TGF β pathway may control interstitial cell proliferation in the neonatal kidney. Although TGF β signaling has been a focus of research in homeostasis of adult interstitial cells, little is known about its function in differentiation of the renal interstitium. TGF β signaling is essential for development of the kidney (Dudley et al., 1995; Ikeya et al., 2010; Oxburgh et al., 2004), and controls formation of both the collecting ducts and nephrons (Brown et al., 2013; Hartwig et al., 2008). Recessive mutations in genes within this signaling pathway have been identified as monogenic causes of Congenital Anomalies of the Kidney and Urinary Tract (CAKUT), indicating that TGF β pathway dysregulation may be an important factor in neonatal kidney disease. An important example is the identification of mutations in bone morphogenetic protein 4 (BMP4) in patients with renal hypodysplasia (Kohl et al., 2014; Weber et al., 2008).

TGF β superfamily ligands signal through two distinct intracellular pathways: Smad, which is initiated by phosphorylation of receptor-associated Smad (R-Smad) transcription factors and mitogen-associated protein kinase (MAPK) which is initiated by the TGF β -associated kinase TAK1 (MAP3K7). Kidneys of mice with conditional inactivation of *Map3k7* in the *Foxd1*

lineage develop spontaneous neonatal mesangiosclerosis (Karolak et al., 2018), suggesting that MAPK is selectively required for mesangial differentiation.

The current study addresses the role of Smad pathway signaling in the *Foxd1* lineage. Phosphorylated R-Smads associate with the common mediator Smad (Smad4) to accumulate in the nucleus. R-Smads and Smad4 bind DNA and interact with a variety of other transcription factors, facilitating highly context-dependent responses. Because Smad4 is unique and essential for Smad-mediated responses, we selected it as a tractable node in the pathway for conditional gene inactivation. We report that *Smad4* controls proliferation within the interstitium of the neonatal kidney by attenuating Wnt signaling.

RESULTS

Loss of Smad4 causes expansion of the renal interstitium

To understand the role of TGF β /BMP in the developing renal interstitium, *Smad4* was inactivated in interstitial cell progenitors using *Foxd1*^{Cre}. To sensitize the strain for cre-mediated recombination, *Foxd1*^{Cre} was combined with one null *Smad4* allele and one loxP-flanked allele (Chu et al., 2004). This cross generates offspring of four genotypes; *Foxd1*^{+/+};*Smad4*^{-/loxP}, *Foxd1*^{+/+};*Smad4*^{+/loxP}, *Foxd1*^{+/Cre};*Smad4*^{+/loxP}, and *Foxd1*^{+/Cre};*Smad4*^{-/loxP}. *Foxd1* is disrupted in the *Foxd1*^{Cre} strain and *Foxd1*^{+/Cre};*Smad4*^{+/loxP} was selected as the control group (referred to as *Smad4*^{con}) to control for any subtle effects of compound heterozygous inactivation of *Foxd1* and *Smad4*. *Foxd1*^{+/Cre};*Smad4*^{-/loxP} is referred to as *Smad4*^{IC}. In this comparison, the *Smad4*^{IC} group is globally heterozygous for *Smad4*. For this study, we used the *Smad4*^{tm1Rob/+} strain in which the first coding exon of *Smad4* is removed (Chu et al., 2004). *Smad4*^{con} mice did not develop any overt phenotypes. *Smad4*^{IC} mice were distinguishable from *Smad4*^{con} littermates at birth because they had kinked tails, and they developed hindlimb paralysis during the first postnatal week. These phenotypes are most likely explained by expression of *Foxd1* in the somite and in the central nervous system (Hatini et al., 1994; Robinton et al., 2019). To avoid confounding effects of hindlimb paralysis on postnatal kidney development, analyses were carried out at embryonic time points up to postnatal day 1 (P1).

To evaluate the efficiency of cre recombination, we first compared *Smad4* transcript levels, and found that they are reduced by approximately 60% in *Smad4^{IC}* kidneys versus *Smad4^{con}* (Fig. 1A). To measure recombination efficiency specifically in the *Foxd1* lineage, we selected cells expressing the interstitial cell surface marker PDGFR α (Fig. S1A,B), and single-cell genotyped them (Fig. S1C,D). Figure 1B summarizes the frequency of recombination of interstitial cells in the *Smad4^{IC}* genetic model; 87.1% of cells were recombined at the *Smad4* locus and thus null for *Smad4*.

To determine if loss of *Smad4* in the *Foxd1*-expressing interstitial cell progenitor affects lineage commitment, we introduced the *Rosa26R* reporter gene. The localization of *Foxd1* lineage cells in the *Smad4^{IC};Rosa26R* strain is indistinguishable from *Smad4^{con};Rosa26R*, and thus we conclude that lineage commitment is unperturbed (Fig. S2). Transverse sections were cut through the center of the kidney to reveal the cortex and medulla. The cortex contains glomeruli, while the medulla does not. The medulla is divided into an outer medulla directly adjacent to the cortex and an inner medulla or papilla that extends into the pelvis of the kidney. For clarity, we refer to three distinct regions: cortex, outer medulla, and papilla (equivalent to inner medulla). Compared with *Smad4^{con}*, *Smad4^{IC}* shows abundant stroma in the outer medulla and papilla, and a paucity of epithelial structures in both of these zones (Fig. 1C,D). The R26R reporter serves as a helpful marker that can be used in parallel with histological analysis to understand the abundance of *Foxd1* lineage cells. Comparison of *Smad4^{con}* (Fig. 1 E-J) and *Smad4^{IC}* (Fig. 1K-P) revealed a marked expansion of *Foxd1*-lineage interstitium which was regionalized in the tissue; a modest difference was noted in cortical interstitium (Fig. 1H,N), while pronounced pockets of stroma were seen in the outer medulla and papilla (Fig. 1I,J,O,P). We conclude that *Smad4* is required in the *Foxd1* lineage for appropriate formation of the renal interstitium.

Smad4 is required for appropriate differentiation of interstitial cells

During renal development, interstitial cells transition from a FOXD1/PDGFR α double-positive state in the cortex to a α -SMA/PDGFR β double-positive state in the outer medulla. To determine if the stromal expansion observed in *Smad4^{IC}* mice is associated with impaired interstitial cell differentiation, expression of the interstitial markers α -SMA and PDGFR β were examined in kidneys from embryonic and postnatal mice. Though comparable to control at E17.5 (Fig. S3), differences in α -SMA and PDGFR β expression are observed in *Smad4^{IC}* mouse kidneys by P0.

Smad4^{IC} mice display reduced α -SMA expression in the outer medulla compared to control (Fig. 2A,B). In contrast, PDGFR β expression is increased in both the outer medulla and papilla of *Smad4^{IC}* mice compared to control (Fig. 2C,D). Confirming these findings, immunoblots of lysates from whole kidneys (Fig. 2E) showed a significant increase of PDGFR β (Fig. 2F) and decrease of α -SMA (Fig. 2G) in *Smad4^{IC}* mice. The lack of expression of α -SMA in the abundant *Foxd1*-derived interstitial cells of the outer medulla suggests that *Smad4* is required for appropriate expression of their differentiation program.

Loss of Smad4 from the Foxd1 lineage causes features of collecting duct compression and urine outflow occlusion

One possible explanation for the pockets of interstitial cells seen in the *Smad4^{IC}* medulla is that collecting duct (CD) organization is impaired, causing aberrant clustering of interstitial cells, and to determine if this was the case, we compared *Smad4^{IC}* kidney tissue with controls using two strategies. Three dimensional modeling of whole kidneys stained with the CD marker TROMA1 showed that branching at embryonic day 14.5 is indistinguishable between *Smad4^{con}* and *Smad4^{IC}* mice (Fig. 3A-C, S4A,B). Studies of kidney development using the *Smad4^{tm1Mak}* strain which has a deletion in the carboxy-terminal domain of SMAD4 (Sirard et al., 1998) have determined a 12% increase in number of collecting duct branch-points in heterozygotes at E13.5 (Hartwig et al., 2005). The fact that we do not observe any difference between *Smad4^{con}* and *Smad4^{IC}* indicates that this phenotype of global *Smad4* modification is not reproduced with the *Smad4^{tm1Rob/+}* strain used in this study. To analyze collecting ducts at P0 when the kidney is too large for modeling based on whole mount immunostaining, we sectioned through the longitudinal plane of the kidney perpendicular to the papilla to obtain transverse sections of the papilla where collecting ducts are closely bundled (Fig. 3D), and immunostained these sections. We found a reduced number of patent TROMA1-positive structures in the papilla of *Smad4^{IC}* mice compared to *Smad4^{con}* (Fig. 3E,F). High magnification images of the papilla revealed TROMA1-positive tubules with an atypical compressed morphology in *Smad4^{IC}* kidneys (Fig. 3G,H). When quantified, the compressed TROMA1-expressing CDs account for the reduced number of CDs in *Smad4^{IC}* mice (Fig. 3I). We hypothesize that these structures are remnants of functional CDs that are constricted by stromal expansion. CD compression is predicted to cause restricted urine outflow, and consistent with this, *Smad4^{IC}* mutant kidneys displayed nephron

tubule expansion (Fig. 3J-L) and distended Bowman's spaces (Fig. 3M-O). Increased mesangial α -SMA expression (Fig. 3P,Q, S4C,D) and mesangial area (Fig. 3R) indicate early glomerulosclerosis in *Smad4^{IC}* mice. *In vivo* 5-ethynyl-2'-deoxyuridine (EdU) incorporation revealed an increased proliferative index in mesangial cells of the mutant at P0 (Fig. S4E-G), indicating that this defect is mesangioproliferative. Numbers of glomeruli are comparable between *Smad4^{con}* and *Smad4^{IC}* (Fig. S4H), suggesting that the features of increased physiological load that we observed are not due to differences in nephron number. In summary, the histological features that we observed are consistent with CD compression causing increased luminal pressure in the nephron with associated sclerosis of the glomerulus.

Loss of Smad4 affects nuclear accumulation of Smad3 but not Smad1/5/8

To understand if loss of *Smad4* affects nuclear accumulation of R-Smads in regions of medullary interstitial cell expansion, protein localization of Smads was compared in *Smad4^{con}* and *Smad4^{IC}* mouse kidneys. To localize expression in interstitial cells, we co-stained with α SMA. Signal amplification was used to reliably detect α SMA in the *Smad4^{IC}* kidney. After testing multiple different antibodies for receptor Smads, we concluded that nuclear localization of Smad3 is the most sensitive proxy for TGF β signaling and pSmad1/5/8 is the most sensitive for BMP. These assays are not directly comparable with each other because one measures localization of total protein and the other measure localization of a phosphorylated form. However, signal intensity for each is well documented to correlate with cell signaling leading us to conclude that they are valid reporters for TGF β versus BMP signaling. As anticipated, Smad4 was lost from the interstitium of *Smad4^{IC}* mice (Fig. 4 A,B). In addition, Smad3 was strongly reduced in the interstitium of *Smad4^{IC}* kidneys compared to control (Fig. 4C,D), while pSmad1/5/8 levels were only slightly reduced (Fig. 4E,F). These results reveal that TGF β signaling is primarily affected by *Smad4* inactivation.

Smad4^{IC} kidneys are comparable to *Smad4^{con}* at E17.5 but show a phenotype in the newborn, so we were interested to understand if there were dynamic changes in the TGF β pathway at late developmental time points. A developmental time course of gene expression in the kidney has been reported (Challen et al., 2005), and we screened developmental timepoints from E15.5 to P0 for components of the TGF β signaling pathway. We based the selection of pathway genes on the KEGG pathway hsa04350, which includes 91 genes. Of these, 14 were

differentially expressed in the kidney developmental time course. From this transcriptomic analysis, there was no obvious evidence for a coordinated change expression of TGF β pathway components as an equivalent number of genes were up- and downregulated between E17.5 and neonate (Fig. S5).

Interstitial expansion is due to increased proliferation

To determine if aberrant proliferation is responsible for the interstitial expansion observed in *Smad4^{IC}* mice, we performed *in vivo* EdU incorporation at P0 (Fig. 5). To localize proliferating cells in the interstitium, we co-stained tissue with a cocktail of antibodies for α SMA and PDGFR β . These two interstitial cell markers differ strongly in expression level between *Smad4^{IC}* and *Smad4^{con}*, and by detecting both primary antibodies with secondary antibodies conjugated to the same fluorophore we were able to achieve a comparable signal intensity between the two genotypes. While EdU⁺ cycling interstitial cells were largely limited to the cortex and outer medulla in *Smad4^{con}* kidneys, they were abundant in the papilla of *Smad4^{IC}* mice (Fig. 5A,B). 3D modeling and quantification of comparable volumes confirmed a higher proliferation rate in the papillary interstitium of *Smad4^{IC}* mice compared to *Smad4^{con}* (Fig. 5C-E). We conclude that there is a failure of interstitial cell growth restriction in the transition zone between outer medulla and papilla.

Interstitial expansion correlates with aberrant Wnt/ β -catenin signaling

Several lines of evidence indicate that Wnt/ β -catenin signaling is required for interstitial cell maintenance: loss of *Wnt7B* from the collecting duct epithelium or inactivation of β -catenin in interstitial cell precursors both result in medullary hypoplasia (Boivin et al., 2016; Yu et al., 2009). Thus, developmental genetic studies support a model in which collecting duct-derived Wnt drives medullary interstitial cell proliferation through a β -catenin dependent signaling mechanism. We were therefore curious to understand if Wnt/ β -catenin signaling was perturbed in the *Smad4^{IC}* kidney. Expression of the feedback inhibitor axin 2 is a sensitive read-out of Wnt/ β -catenin signaling, and we compared its expression level in *Smad4^{con}* and *Smad4^{IC}* kidneys. *In situ* hybridization revealed axin 2 expression in the interstitium of the outer medulla and papilla of *Smad4^{con}*, but undetectable levels in *Smad4^{IC}* (Figs. 6A,B, S6). Reduction in activation

of feedback inhibitors can be interpreted as evidence of reduced Wnt/ β -catenin signaling, which would be unanticipated considering the proliferative phenotype of *Smad4*^{IC}. We therefore evaluated expression of a panel of other Wnt/ β -catenin targets. LEF1 was elevated in the outer medulla and papillary interstitium of *Smad4*^{IC} kidneys (Fig. 6C-E), along with the Wnt/ β -catenin-activated cell cycle regulator CCND1 (Fig. 6F-H), suggesting an increase in Wnt/ β -catenin signaling and proliferation relative to *Smad4*^{con}. We also found increased expression of the Wnt responsive cell cycle regulator CDKN1C (P57KIP2) (Fig. 6I-K), which is required for renal medulla formation (Yu et al., 2009; Zhang et al., 1997).

DISCUSSION

Considering the central role that *Smad4* plays in TGF β superfamily signaling, it is not surprising that the *Foxd1*^{IC} strain displays a profound phenotype in the neonate. TGF β superfamily signaling in kidney fibroblasts has mainly focused on the study of TGF β ligands, because foundational work showed that they promote proliferation (Roberts et al., 1985), extracellular matrix deposition (Edwards et al., 1987; Ignatz and Massagué, 1986), and myofibroblast transition (Rønnov-Jessen and Petersen, 1993). In previous work, we explored the consequences of inactivating the TGF β /MAPK pathway in interstitial cells by inactivating TGF β -associated kinase 1 (*Map3k7*) using *Foxd1*^{+cre} (Karolak et al., 2018). In this study, we define the consequences of inactivating the TGF β /Smad response by inactivating *Smad4*.

TGF β superfamily ligands promote phosphorylation of the R-Smads 1, 2, 3, and 5 (Ramachandran et al., 2018; Zhang et al., 1996), and therefore one tractable strategy for studying Smad responses is to inactivate *Smad4*, which is required for nuclear retention and transcriptional activity of activated R-Smads (Lagna et al., 1996; Schmierer and Hill, 2005). Unexpectedly, we find that *Smad4* inactivation eliminates nuclear accumulation of the Smad3 transcription factor, while only slightly reducing nuclear accumulation of the Smad1/5 transcription factors. This is in line with the Smad transcriptional response to TGF β 1, which is estimated to be comprised of approximately 75% Smad2/3 transcriptional response and 25% Smad1/5 transcriptional response (Ramachandran et al., 2018). The finding that Smad1/5 nuclear accumulation is not lost indicates that the BMP R-Smad response is only marginally affected by

Smad4 inactivation. Thus, from the perspective of Smad activation, our genetic model reflects the effects of eliminating TGF β rather than BMP signaling.

The number of interstitial cells in the kidney must be carefully balanced both during development and in the adult. In development, interstitial cells provide essential signals that guide differentiation of the surrounding epithelia (Das et al., 2013; Fetting et al., 2014). In the adult, interstitial cells provide essential endocrine functions such as erythropoietin production (Kobayashi et al., 2016), but their uncontrolled expansion is the basis for organ fibrosis in which functional tissue is marginalized (Humphreys et al., 2010). Our observation that reducing TGF β /Smad signaling in the interstitial cell lineage leads to increased proliferation in the neonate agrees with findings from studies of multiple cell lines showing that growth is inhibited by TGF β (Roberts et al., 1985). An interesting feature of our study is that the effect is limited to a particular zone of interstitial cells at the border between outer medulla and papilla. Genetic studies have suggested that formation of the medullary interstitium requires Wnt/ β -catenin signaling and our work indicates that TGF β /Smad signaling inhibits this proliferative stimulus in a regional manner to ensure appropriate structural differentiation of the medulla. Interestingly, the effect of knocking out the Wnt/ β -catenin pathway in the interstitial lineage is loss of the kidney medulla, but the cortex of these kidneys is preserved (Boivin and Bridgewater, 2018; Yu et al., 2009), suggesting specificity of Wnt/ β -catenin for medullary interstitium. Similarly, our inactivation study of *Smad4* reveals over-proliferation of the medullary interstitium, indicating that this Wnt/ β -catenin - TGF β /Smad circuit for growth control primarily affects this region.

Loss of *Smad4* causes differential effects on Wnt/ β -catenin targets, with a loss of expression of the Wnt feedback inhibitor axin 2 and increased LEF1 and p57kip2. This supports a model in which loss of feedback inhibition causes increased Wnt/ β -catenin signaling resulting in increased proliferation. We hypothesize that the loss of feedback inhibition could be a primary event in the deregulation of interstitial cell proliferation. Multiple Wnts including *Wnt4* and *Wnt7b* are expressed in the medullary interstitium (Yu et al., 2009), facilitating combinatorial effects. TGF β sources have been less well studied, but review of the Eurexpress in situ hybridization database shows *Tgf β 1* expression in the medulla. Recent single cell expression analysis of E18.5 kidneys has shown a spatial intersection of Lef1 expression with expression of the TGF β -induced transcript TGF β 1i1, supporting a model in which Wnt/ β -catenin mediated

proliferation may be controlled by TGF β (England et al., 2020). Relative amplitudes of these different signaling pathways could be regulated at the level of the ligands or perhaps more likely by other intracellular signaling components or distinct signaling pathways.

In aggregate, our findings suggest that Smads and Wnt/ β -catenin antagonistically control cell proliferation in the medullary interstitium and that the balance of these signaling pathways determines interstitial cell abundance in the postnatal kidney. Understanding this molecular crosstalk will not only contribute important concepts to the pathogenesis of CAKUT, but may also identify therapeutically tractable mechanisms that control kidney fibrosis in the adult.

MATERIALS AND METHODS

Mouse Strains

Animal care was in accordance with the National Research Council Guide for the Care and use of laboratory animals and protocols were approved by the Institutional Animal Care and Use Committee of Maine Medical Center. The second exon that includes the transcriptional start site is targeted in *Smad4*^{tm1Rob/+} (referred to as *Smad4*^{+/-}) and *Smad4*^{tm1.1Rob/tm1.1Rob} (referred to as *Smad4*^{loxP/loxP}) mice (Chu et al., 2004). *Foxd1*^{+/-Cre};*Smad4*^{+/-} mice were crossed to *Smad4*^{loxP/loxP} mice to produce *Foxd1*^{+/-Cre};*Smad4*^{+/-loxP} (*Smad4*^{con}) and *Foxd1*^{+/-Cre};*Smad4*^{-/-loxP} (*Smad4*^{IC}) mice. *Foxd1*^{+/-Cre};*Smad4*^{+/-} and *Smad4*^{loxP/loxP} mice were maintained on an ICR background. *R26RlacZ* mice were maintained on an FVB/NJ background.

Reagents

A complete list of antibodies including source, clone name, product number and application are listed in Supplementary Table 1.

Immunoblotting

Total protein was extracted from whole kidneys as previously described (Blank et al., 2009). Immunoblotting was performed using standard procedures. Antibodies used were anti- α -SMA (1:1000 Sigma), anti-PDGFR β (1:1000 Abcam), anti-Smad4 (1:1000, Santa Cruz) and anti- β -tubulin (1:5,000, Santa Cruz). Protein levels were quantified using FIJI/Image-J software by

measuring the integrated density of the indicated proteins normalized to the β -tubulin loading control.

Whole mount immunofluorescence

E14.5 and P0 kidneys were fixed in 4% PFA at room temperature for 10 or 30 minutes, respectively, then transferred to 70% ethanol at -20°C for storage. P0 kidneys were longitudinally or transversely vibratome-sectioned at 100microns directly in 70% ethanol. Whole kidneys and kidney sections were rehydrated in PBS then permeabilized with 1% Triton-X in PBS for 10 min at 4°C. Tissue was washed with PBS to remove residual detergent then incubated in blocking solution (0.01% Tween in PBS plus 5% serum of secondary antibody species) for 1 h. Lectins Dolichos Biflorus Agglutinin (DBA; Vector Laboratories) and Lotus Tetragonolobus Lectin (LTL; Vector Laboratories) were diluted 1:200 and primary antibodies anti- α -SMA-Cy3 (Sigma), anti-PDGFR β (Abcam), anti-cytokeratin8/TROMA-1 (DSHB), anti-LEF1 (Cell Signaling), anti-BRN1 (Santa Cruz Biotechnology), anti-AnnexinA2 (Cell Signaling), p57kip2 (Cell Signaling), anti-CyclinD1 (Cell Signaling), and anti-ki67 (Abcam), were diluted 1:50 in blocking solution. Tyramide Signal Amplification (TSA; PerkinElmer) was used according to the manufacturer's protocol for whole mount immunostaining with anti-Smad4 (1:500; Santa Cruz), anti-Smad3 (1:3,000; Cell Signaling) and anti-pSmad1/5/8 (1:1000; V. Lindner) antibodies. Blocked tissue was incubated in diluted lectins/primary antibodies for 24hr at 4°C followed by three washes with blocking solution, the third wash for 24hr at 4°C. Alexa-Fluor 488/568/647 secondary antibodies (Molecular Probes) were used at 1:200 and incubated for 24hr followed by three washes with 0.01% Tween in PBS, the third wash for 24hr at 4°C. Tissue was counterstained with DAPI (1:5,000), dehydrated in ethanol, and cleared with BABB (1:1 benzyl alcohol:benzyl benzoate) before imaging with a laser scanning confocal microscope.

***In situ* hybridization**

P0 kidneys were fixed in 4% PFA overnight at 4°C, washed with PBS for 4hr, then equilibrated in 30% sucrose/PBS overnight at 4°C. After flash freezing in OCT, kidneys were cryosectioned at 20 microns and sections were fixed in 4% PFA for 10 min, rinsed three times with PBS, incubated in 20ug/ml proteinase K in PBS for 10 minutes, followed by three rinses with PBS. Sections were incubated in 1.3% triethylamine;0.375% acetic anhydride for 10 minutes, rinsed

three times with PBS then incubated in hybridization buffer for 2hr. DIG-labeled axin 2 sense versus antisense riboprobes (Jho et al., 2002) were diluted to 500ng/ml in hybridization buffer (50% formamide, 5X SSC pH 4.5, 1% SDS, 50ug/ml yeast tRNA, 50ug/ml heparin) and sections were hybridized in a humidified chamber at 68°C overnight. After two washes with 0.2X SSC for 30 min at 72°C, sections were rinsed with NTT (0.15 M NaCl, 0.1% Tween-20, 0.1M Tris-HCl pH 7.5), incubated in blocking buffer (5% heat-inactivated sheep serum, 2% blocking reagent in NTT) for 2 hours, followed by incubation in anti-DIG AP conjugated antibody (diluted 1:4,000 in blocking buffer) overnight at 4°C. After three washes with NTT for 30 min each, sections were rinsed with NTTML (0.15 M NaCl, 0.1% Tween-20, 0.1M Tris-HCl pH 9.5, 50mM MgCl₂, 2mM levamisole) then incubated in BM purple until desired staining was reached. Stained sections were rinsed three times with PBS then mounted in glycerol for imaging.

***In vivo* proliferation analysis**

One EdU pulse (20mg/kg) was administered to P0 pups by intraperitoneal injection. After 2hr, kidneys were dissected on ice and fixed in 4% PFA for 30 min. Kidneys were vibratome sectioned and whole mount immunofluorescence staining was performed as described above. Click-it chemistry was subsequently performed on sections according to the manufacturer protocol (ThermoFisher) followed by imaging with a laser scanning confocal microscope. EdU quantification was performed with Imaris image analysis software (Bitplane). Briefly, equivalent 250x250x50 μm^3 image areas were selected in the outer medulla and papilla and the spot function was used to count EdU⁺ nuclei. A filter was applied to the spot function to select for PDGFR β / α -SMA-labeled interstitial cells. Equivalent image analysis, including identical thresholding, was performed on six biological replicates ($n=6$).

Histology and detection of beta-gal activity

Paraffin-embedding and H&E staining of tissue was performed by the Maine Medical Center Research Institute Histomorphometry Core. For X-gal staining, whole P0 kidneys were vibratome sectioned (300 μm), rinsed in X-gal buffer (5mM EGTA; 2mM MgCl₂; 0.02% NP40; 250 μM sodium deoxycholate in PBS) then fixed for 30 minutes (1% formaldehyde; 0.2% glutaraldehyde in X-gal buffer). Sections were washed 2X 10 mins with X-gal buffer then stained (5mM K₃Fe; 5mM K₄Fe; 0.5mg/ml X-gal in X-gal buffer) overnight at 37°C. Stained

sections were washed 2X 10 mins with X-gal buffer then dehydrated through ethanol/xylenes. Dehydrated sections were embedded in paraffin then re-sectioned at 10µm and counter stained with Nuclear Fast Red.

Single cell recombination analysis

Nephrogenic zone cells (NZCs) were isolated from E17.5 *Smad4^{IC}* mice as previously described (Brown et al., 2015) and labeled with PE-conjugated mouse anti-CD140a/PDGFR α (1:10 Miltenyi) followed by incubation with Anti-PE MicroBeads (1:20 Miltenyi). Labeled cells were purified by three rounds of magnetic-activated cell sorting (MACS) and single cells were manually picked from the PE-positive fraction with the aid of an EVOS digital microscope. Total DNA was amplified from single cells with the REPLI-g Single Cell Kit (Qiagen) and genotyping was performed with NovaTaq Hot Start Master Mix (Millipore) according to the manufacturer's cycling parameters ($T_m=55^{\circ}\text{C}$) and the primers listed in Supplementary Table 2.

Statistical Analysis

Chi-Square testing was performed to verify that all data sets were normally distributed. Two-tailed T-tests were performed comparing normally distributed groups with $p>0.05$ considered significant. Proliferation analysis of FH535-treated mice and FH535-treated monolayer cells were subject to one-way ANOVA. Asterisks indicate statistical significance as follows: not significant (ns)= $p>0.05$; *= $p<0.05$; **= $p<0.01$; ***= $p<0.00$.

ACKNOWLEDGEMENTS

The authors gratefully acknowledge Dr. Volkhard Lindner for providing the pSmad1/5/8 antibody and the MMCRI Histomorphometry Core for tissue processing and H&E and CD31 staining. The authors also thank Drs. Lucy Liaw, Calvin Vary, Pradeep Sathyanaryana and Ron Korstanje for their critical review of this manuscript.

COMPETING INTERESTS

The authors declare no competing financial interests.

FUNDING

The project described was supported by the National Institutes of Health grant R24DK106743 and RC2DK125960 to L.O. and F31DK112602 to SSM. The content is solely the responsibility of the authors and does not necessarily represent the official views of the National Institutes of Health.

REFERENCES

- Blank, U., Brown, A., Adams, D.C., Karolak, M.J., Oxburgh, L., 2009. BMP7 promotes proliferation of nephron progenitor cells via a JNK-dependent mechanism. *Development (Cambridge, England)* 136, 3557-3566.
- Boivin, F.J., Bridgewater, D., 2018. beta-catenin in stromal progenitors controls medullary stromal development. *American journal of physiology. Renal physiology*.
- Boivin, F.J., Sarin, S., Dabas, P., Karolak, M., Oxburgh, L., Bridgewater, D., 2016. Stromal beta-catenin overexpression contributes to the pathogenesis of renal dysplasia. *The Journal of pathology* 239, 174-185.
- Brown, A.C., Muthukrishnan, S.D., Guay, J.A., Adams, D.C., Schafer, D.A., Fetting, J.L., Oxburgh, L., 2013. Role for compartmentalization in nephron progenitor differentiation. *Proceedings of the National Academy of Sciences of the United States of America* 110, 4640-4645.
- Brown, A.C., Muthukrishnan, S.D., Oxburgh, L., 2015. A synthetic niche for nephron progenitor cells. *Developmental cell* 34, 229-241.
- Challen, G., Gardiner, B., Caruana, G., Kostoulas, X., Martinez, G., Crowe, M., Taylor, D.F., Bertram, J., Little, M., Grimmond, S.M., 2005. Temporal and spatial transcriptional programs in murine kidney development. *Physiological genomics* 23, 159-171.
- Chu, G.C., Dunn, N.R., Anderson, D.C., Oxburgh, L., Robertson, E.J., 2004. Differential requirements for Smad4 in TGFbeta-dependent patterning of the early mouse embryo. *Development (Cambridge, England)* 131, 3501-3512.
- Das, A., Tanigawa, S., Karner, C.M., Xin, M., Lum, L., Chen, C., Olson, E.N., Perantoni, A.O., Carroll, T.J., 2013. Stromal-epithelial crosstalk regulates kidney progenitor cell differentiation. *Nature cell biology* 15, 1035-1044.
- Dudley, A.T., Lyons, K.M., Robertson, E.J., 1995. A requirement for bone morphogenetic protein-7 during development of the mammalian kidney and eye. *Genes & development* 9, 2795-2807.
- Edwards, D.R., Murphy, G., Reynolds, J.J., Whitham, S.E., Docherty, A.J., Angel, P., Heath, J.K., 1987. Transforming growth factor beta modulates the expression of collagenase and metalloproteinase inhibitor. *The EMBO journal* 6, 1899-1904.
- England, A.R., Chaney, C.P., Das, A., Patel, M., Malewska, A., Armendariz, D., Hon, G.C., Strand, D.W., Drake, K.A., Carroll, T.J., 2020. Identification and characterization of cellular heterogeneity within the developing renal interstitium. *Development (Cambridge, England)* 147.

Fetting, J.L., Guay, J.A., Karolak, M.J., Iozzo, R.V., Adams, D.C., Maridas, D.E., Brown, A.C., Oxburgh, L., 2014. FOXD1 promotes nephron progenitor differentiation by repressing decorin in the embryonic kidney. *Development (Cambridge, England)* 141, 17-27.

Hartwig, S., Bridgewater, D., Di Giovanni, V., Cain, J., Mishina, Y., Rosenblum, N.D., 2008. BMP receptor ALK3 controls collecting system development. *J Am Soc Nephrol* 19, 117-124.

Hartwig, S., Hu, M.C., Cella, C., Piscione, T., Filmus, J., Rosenblum, N.D., 2005. Glypican-3 modulates inhibitory Bmp2-Smad signaling to control renal development in vivo. *Mechanisms of development* 122, 928-938.

Hatini, V., Huh, S.O., Herzlinger, D., Soares, V.C., Lai, E., 1996. Essential role of stromal mesenchyme in kidney morphogenesis revealed by targeted disruption of Winged Helix transcription factor BF-2. *Genes & development* 10, 1467-1478.

Hatini, V., Tao, W., Lai, E., 1994. Expression of winged helix genes, BF-1 and BF-2, define adjacent domains within the developing forebrain and retina. *J Neurobiol* 25, 1293-1309.

Humphreys, B.D., Lin, S.L., Kobayashi, A., Hudson, T.E., Nowlin, B.T., Bonventre, J.V., Valerius, M.T., McMahon, A.P., Duffield, J.S., 2010. Fate tracing reveals the pericyte and not epithelial origin of myofibroblasts in kidney fibrosis. *American Journal of Pathology* 176, 85-97.

Ignatz, R.A., Massagué, J., 1986. Transforming growth factor-beta stimulates the expression of fibronectin and collagen and their incorporation into the extracellular matrix. *The Journal of biological chemistry* 261, 4337-4345.

Ikeya, M., Fukushima, K., Kawada, M., Onishi, S., Furuta, Y., Yonemura, S., Kitamura, T., Nosaka, T., Sasai, Y., 2010. Cv2, functioning as a pro-BMP factor via twisted gastrulation, is required for early development of nephron precursors. *Developmental biology* 337, 405-414.

Inazaki, K., Kanamaru, Y., Kojima, Y., Sueyoshi, N., Okumura, K., Kaneko, K., Yamashiro, Y., Ogawa, H., Nakao, A., 2004. Smad3 deficiency attenuates renal fibrosis, inflammation, and apoptosis after unilateral ureteral obstruction. *Kidney international* 66, 597-604.

Jho, E.H., Zhang, T., Domon, C., Joo, C.K., Freund, J.N., Costantini, F., 2002. Wnt/beta-catenin/Tcf signaling induces the transcription of Axin2, a negative regulator of the signaling pathway. *Molecular and cellular biology* 22, 1172-1183.

Karolak, M.J., Guay, J.A., Oxburgh, L., 2018. Inactivation of MAP3K7 in FOXD1-expressing cells results in loss of mesangial PDGFRBeta and juvenile kidney scarring. *American journal of physiology. Renal physiology* 315, F336-f344.

Kobayashi, H., Liu, Q., Binns, T.C., Urrutia, A.A., Davidoff, O., Kapitsinou, P.P., Pfaff, A.S., Olauson, H., Wernerson, A., Fogo, A.B., Fong, G.H., Gross, K.W., Haase, V.H., 2016. Distinct subpopulations of FOXD1 stroma-derived cells regulate renal erythropoietin. *The Journal of clinical investigation* 126, 1926-1938.

Kohl, S., Hwang, D.Y., Dworschak, G.C., Hilger, A.C., Saisawat, P., Vivante, A., Stajic, N., Bogdanovic, R., Reutter, H.M., Kehinde, E.O., Tasic, V., Hildebrandt, F., 2014. Mild recessive mutations in six Fraser syndrome-related genes cause isolated congenital anomalies of the kidney and urinary tract. *J Am Soc Nephrol* 25, 1917-1922.

Lagna, G., Hata, A., Hemmati-Brivanlou, A., Massagué, J., 1996. Partnership between DPC4 and SMAD proteins in TGF-beta signalling pathways. *Nature* 383, 832-836.

Morishita, Y., Yoshizawa, H., Watanabe, M., Ishibashi, K., Muto, S., Kusano, E., Nagata, D., 2014. siRNAs targeted to Smad4 prevent renal fibrosis in vivo. *Scientific reports* 4, 6424.

Oxburgh, L., Chu, G.C., Michael, S.K., Robertson, E.J., 2004. TGFbeta superfamily signals are required for morphogenesis of the kidney mesenchyme progenitor population. *Development (Cambridge, England)* 131, 4593-4605.

Ramachandran, A., Vizán, P., Das, D., Chakravarty, P., Vogt, J., Rogers, K.W., Müller, P., Hinck, A.P., Sapkota, G.P., Hill, C.S., 2018. TGF- β uses a novel mode of receptor activation to phosphorylate SMAD1/5 and induce epithelial-to-mesenchymal transition. *eLife* 7, e31756.

Roberts, A.B., Anzano, M.A., Wakefield, L.M., Roche, N.S., Stern, D.F., Sporn, M.B., 1985. Type beta transforming growth factor: a bifunctional regulator of cellular growth. *Proceedings of the National Academy of Sciences of the United States of America* 82, 119-123.

Robinton, D.A., Chal, J., Lummertz da Rocha, E., Han, A., Yermalovich, A.V., Oginuma, M., Schlaeger, T.M., Sousa, P., Rodriguez, A., Urbach, A., Pourquié, O., Daley, G.Q., 2019. The Lin28/let-7 Pathway Regulates the Mammalian Caudal Body Axis Elongation Program. *Developmental cell* 48, 396-405.e393.

Rønnov-Jessen, L., Petersen, O.W., 1993. Induction of alpha-smooth muscle actin by transforming growth factor-beta 1 in quiescent human breast gland fibroblasts. Implications for myofibroblast generation in breast neoplasia. *Laboratory investigation; a journal of technical methods and pathology* 68, 696-707.

Schmierer, B., Hill, C.S., 2005. Kinetic analysis of Smad nucleocytoplasmic shuttling reveals a mechanism for transforming growth factor beta-dependent nuclear accumulation of Smads. *Molecular and cellular biology* 25, 9845-9858.

Sirard, C., de la Pompa, J.L., Elia, A., Itie, A., Mirtsos, C., Cheung, A., Hahn, S., Wakeham, A., Schwartz, L., Kern, S.E., Rossant, J., Mak, T.W., 1998. The tumor suppressor gene Smad4/Dpc4 is required for gastrulation and later for anterior development of the mouse embryo. *Genes & development* 12, 107-119.

Weber, S., Taylor, J.C., Winyard, P., Baker, K.F., Sullivan-Brown, J., Schild, R., Knuppel, T., Zurowska, A.M., Caldas-Alfonso, A., Litwin, M., Emre, S., Ghiggeri, G.M., Bakkaloglu, A., Mehls, O., Antignac, C., Network, E., Schaefer, F., Burdine, R.D., 2008. SIX2 and BMP4 mutations associate with anomalous kidney development. *J Am Soc Nephrol* 19, 891-903.

Yu, J., Carroll, T.J., Rajagopal, J., Kobayashi, A., Ren, Q., McMahon, A.P., 2009. A Wnt7b-dependent pathway regulates the orientation of epithelial cell division and establishes the cortico-medullary axis of the mammalian kidney. *Development (Cambridge, England)* 136, 161-171.

Zhang, P., Liégeois, N.J., Wong, C., Finegold, M., Hou, H., Thompson, J.C., Silverman, A., Harper, J.W., DePinho, R.A., Elledge, S.J., 1997. Altered cell differentiation and proliferation in mice lacking p57KIP2 indicates a role in Beckwith-Wiedemann syndrome. *Nature* 387, 151-158.

Zhang, Y., Feng, X., We, R., Derynck, R., 1996. Receptor-associated Mad homologues synergize as effectors of the TGF-beta response. *Nature* 383, 168-172.

Figures

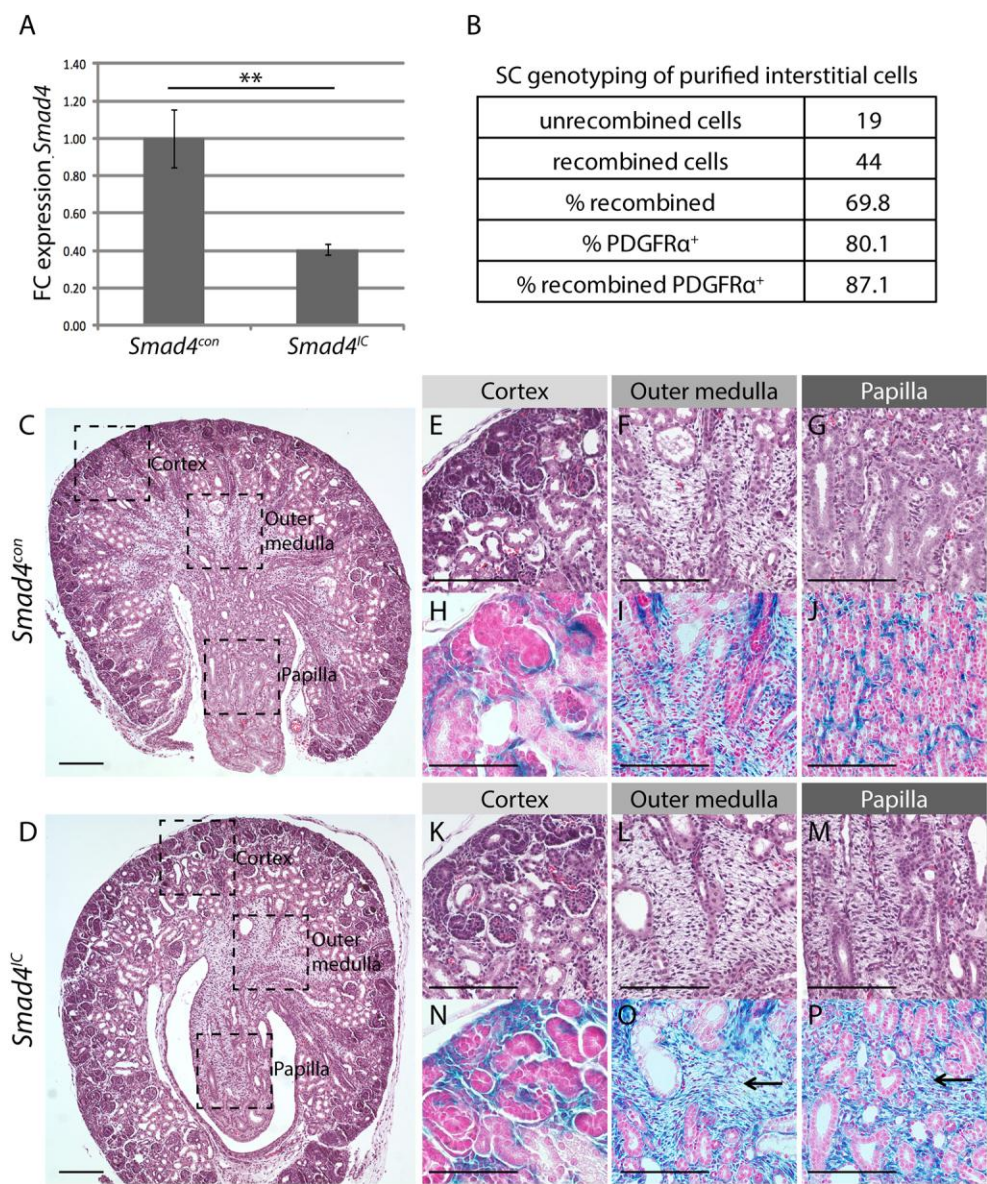


Figure 1. Single cell recombination analysis and histology of *Smad4^{con}* and *Smad4^{IC}* postnatal kidneys. (A) *Smad4* transcript levels in whole kidneys isolated from *Smad4^{con}* and *Smad4^{IC}* P0 mice (**=p<0.01; n=6). FC = fold change; transcript levels normalized to *Smad4^{con}* \pm SEM from three separate experiments are graphed. (B) Summary of recombination frequency in purified cortical interstitial cells. (C, D) Transverse kidney sections with boxes showing

regions of cortex, outer medulla and papilla shown at higher magnification in panels E-P. (E, F, G) Representative H&E fields of *Smad4^{con}* kidneys. (H, I, J) Representative fields of X-Gal-stained sections from kidneys of *Smad4^{con}* on the R26R background. (K, L, M) Representative H&E fields of *Smad4^{IC}* kidneys. (H, I, J) Representative fields of X-Gal-stained sections from kidneys of *Smad4^{IC}* on the R26R background. Arrows denote X-Gal-positive regions of expanded stroma. Scale bars: 200µm in C, D; 100µm in E-P.

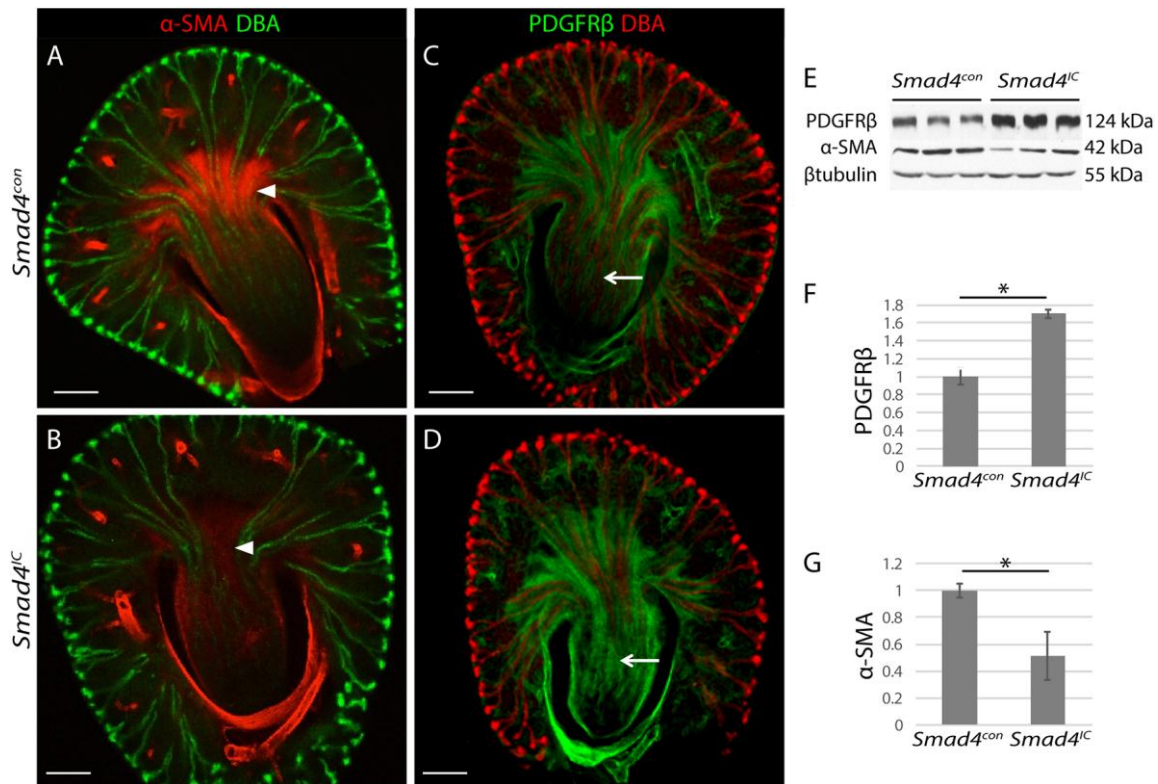


Figure 2. *Smad4* is required for differentiation of the renal interstitium. Whole mount immunofluorescence of kidney vibratome sections representative of 6 *Smad4*^{con} and 6 *Smad4*^{IC} kidneys stained with DBA and α -SMA (A, B) or PDGFR β (C, D). Arrowheads mark comparable regions of outer medulla stroma and arrows indicate comparable regions of papillary stroma in *Smad4*^{con} and *Smad4*^{IC}. (E) Immunoblots of whole kidney lysates from three *Smad4*^{con} and three *Smad4*^{IC} mice probed with α -SMA, PDGFR β , and β -tubulin antibodies. (F) Quantification of band intensities for PDGFR β . (G) Quantification of band intensities for α -SMA. Error bars are SEM and represent three independent experiments. *=p<0.05. Scale bars: 200 μ m.

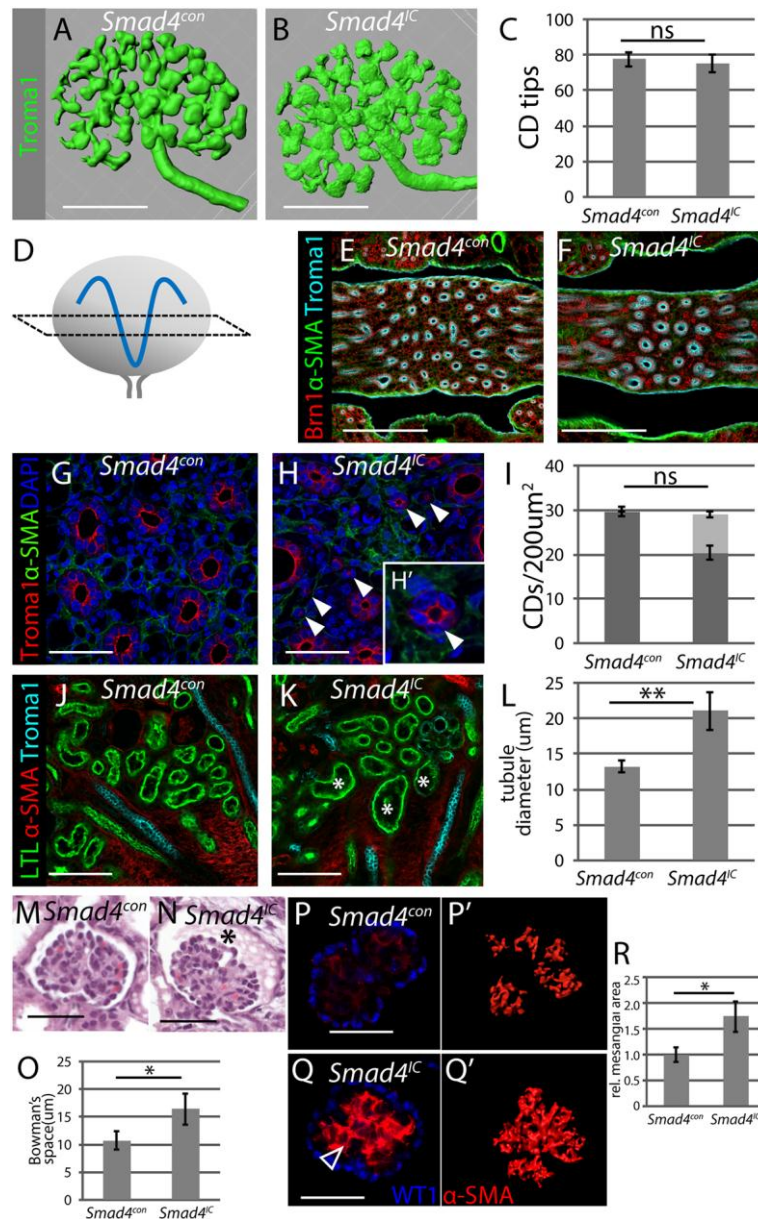


Figure 3. Interstitial expansion results in collecting duct constriction, tubular distension, and expansion of Bowman's space. 3-D reconstruction of E14.5 kidneys from *Smad4*^{con} (A) and *Smad4*^{IC} (B) mice stained for Troma1. (C) Quantification of collecting duct tip number per E14.5 kidney (n=6). (D) Schematic of sectioning plane used for P0 collecting duct analysis. (E, F) P0 kidney vibratome sections stained with Brn1, α -SMA, Troma1. (G, H) P0 kidney vibratome sections stained with α -SMA, Troma1, DAPI. Arrowheads mark abnormally dimensioned Troma-1⁺ collecting ducts. (I) Quantification of collecting ducts per 200 μ m² papilla

(n=6). Dark grey denotes TromaI-stained tubules with clearly patent lumens, while light grey denotes Troma-I-stained tubules with lumens that are not visibly patent. (J, K) P0 kidney vibratome sections stained with LTL, α -SMA, Troma1. Asterisks mark distended proximal tubules. (L) Quantification of LTL+ proximal tubule diameter (n=6). (M, N) Representative sections of glomeruli. Asterisk denotes distended Bowman's space. (O) Quantification of Bowman's space from 6 individual kidneys of each genotype. Only glomeruli that sectioned through the center were counted. (P, Q) Representative sections through P0 glomeruli co-stained with WT1 and α -SMA. Arrowhead marks increased mesangial α -SMA expression. (P', Q') Maximal intensity projections of Z-stacks through glomeruli immunostained with α -SMA. (R) Relative mesangial area normalized to *Smad4*^{con} (μm^2 ; n=6) of glomeruli from *Smad4*^{con}. *= $p < 0.05$; **= $p < 0.01$. Scale bars: 200 μm in A-F; 50 μm in G-K; 20 μm in M-P.

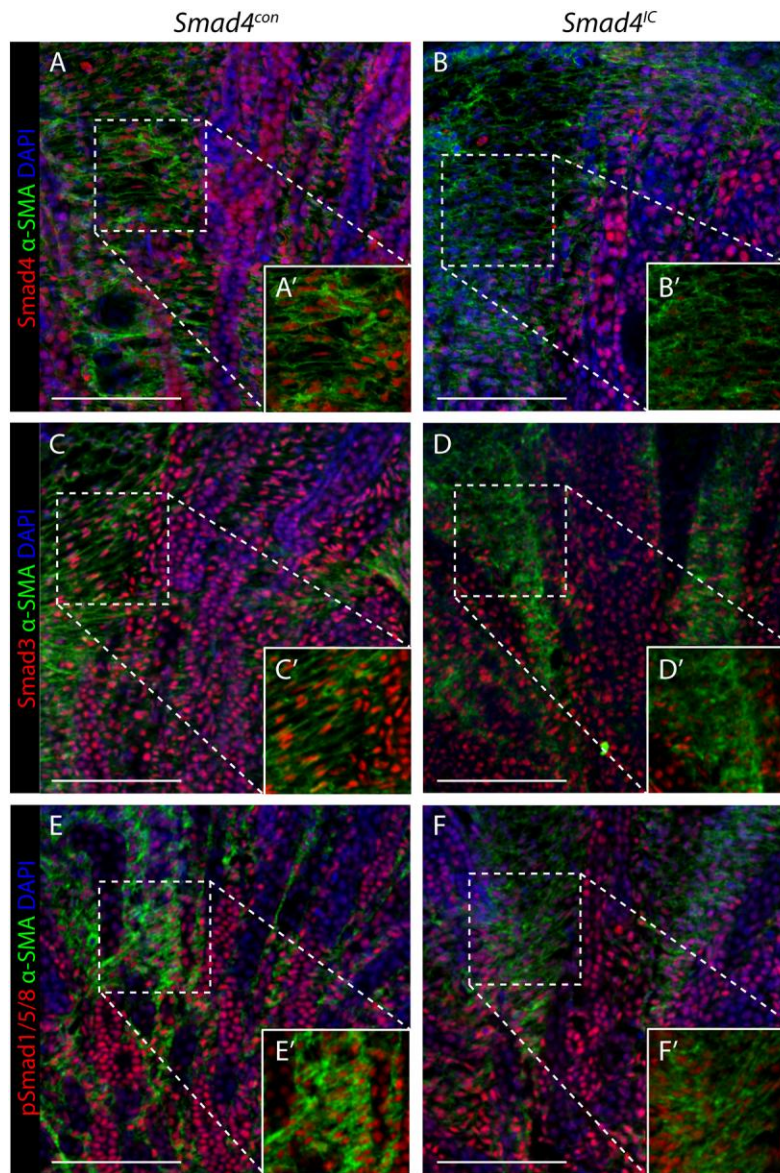


Figure 4. Nuclear Smad3, but not Smad1/5/8, is decreased in the interstitium of *Smad4^{IC}* mice. Immunofluorescence with Tyramide Signal Amplification (TSA) of P0 kidneys from *Smad4^{con}* (A, C, E) and *Smad4^{IC}* (B, D, F) mice stained with antibodies recognizing α -SMA (green), DAPI (blue) and Smad4 (A, B), Smad3 (C, D) or pSmad1/5/8 (E, F); n=6. Scale bars: 100 μ m.

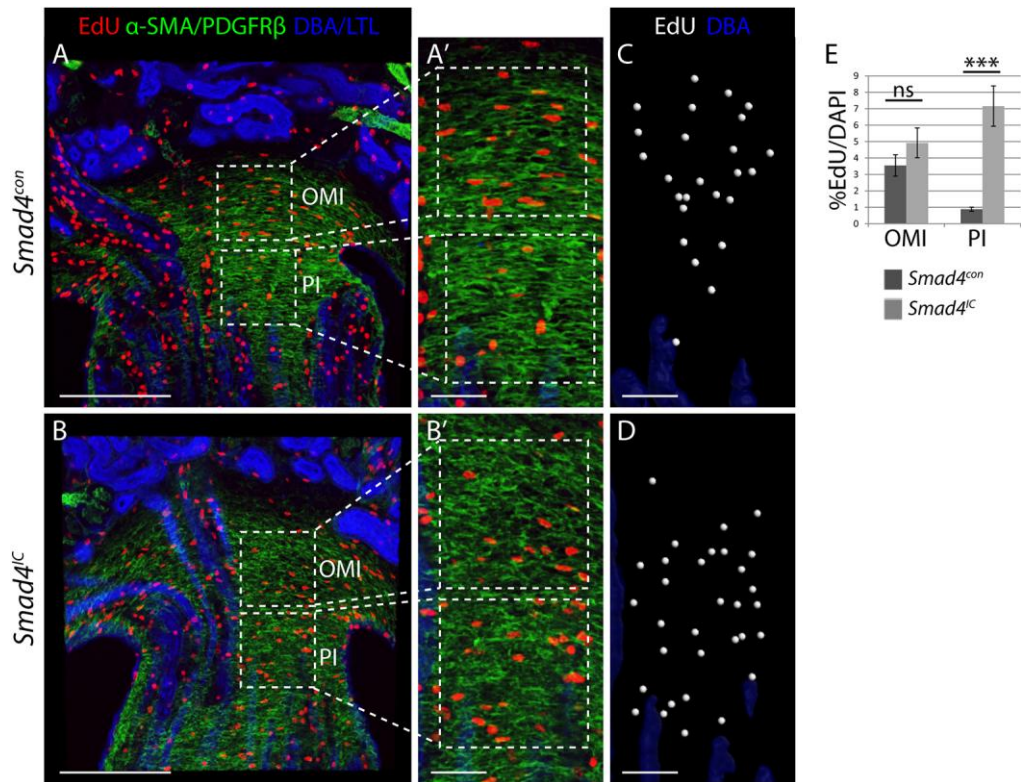


Figure 5. Loss of *Smad4* leads to increased interstitial proliferation. EdU labeling of kidney sections co-stained with collecting duct marker DBA, proximal tubule marker LTL, and α -SMA/PDGFR β from *Smad4^{con}* (A, A') and *Smad4^{IC}* (B, B') mice. (C, D) Three-dimensional tissue analysis of EdU⁺ cells in hatched volumes of the outer medullary interstitium (OMI) and papillary interstitium (PI) using Imaris software. (E) Quantification of 3-D analysis showing %EdU⁺/DAPI⁺ interstitial cells in the hatched volumes of OMI and IMI of *Smad4^{con}* and *Smad4^{IC}* mice; n=6. ns=p>0.05; ***=p<0.001. Scale bars: 200 μ m in A, B; 50 μ m in A', B', C, D.

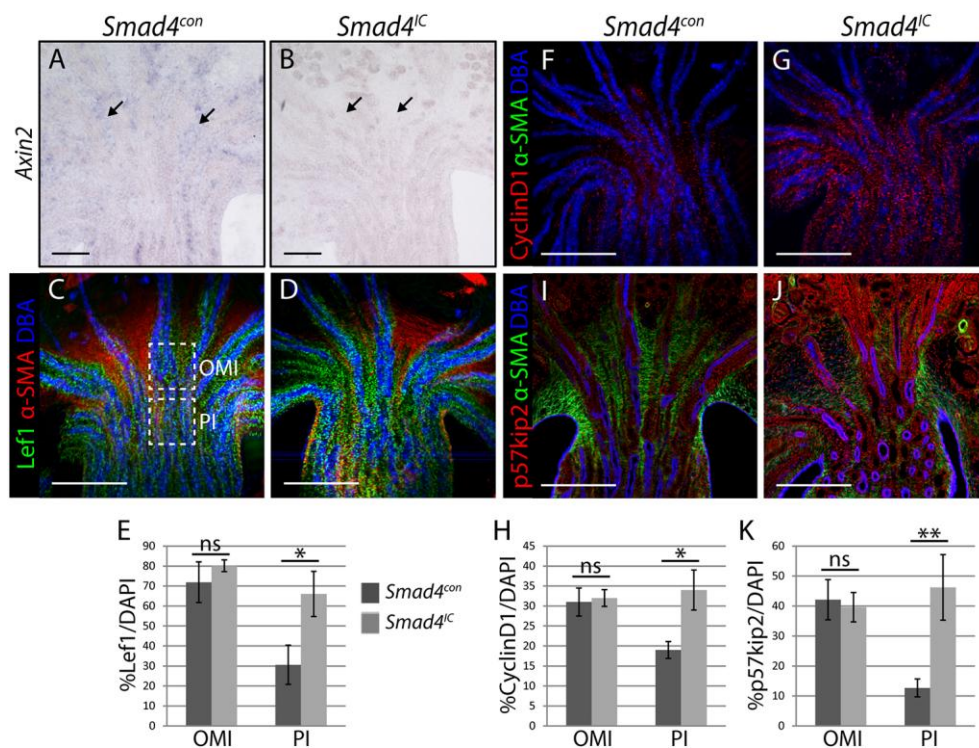


Figure 6. Increased proliferation is associated with aberrant Wnt signaling. (A, B) Axin 2 *in situ* hybridization on P0 kidneys from *Smad4*^{con} (A) and *Smad4*^{IC} (B) mice. Immunofluorescent staining of vibratome sections of P0 kidneys from *Smad4*^{con} (C, F, I) and *Smad4*^{IC} (D, G, J) mice stained with antibodies recognizing α-SMA and DBA combined with either LEF1 (C, D), CyclinD1 (F, G) or p57kip2 (I, J). (E-K) Quantification of numbers of stained cells in the outer medullary interstitium (OMI) and papillary interstitium (PI) of immunostained sections. Examples of regions selected for quantification are shown in panel C. (E) Quantification of LEF1⁺/DAPI⁺ (n=6), (H) Quantification of CyclinD1⁺/DAPI⁺ (n=6) (K) Quantification of p57kip2⁺/DAPI⁺ (n=6). Scale bars: 200μm in A-J.

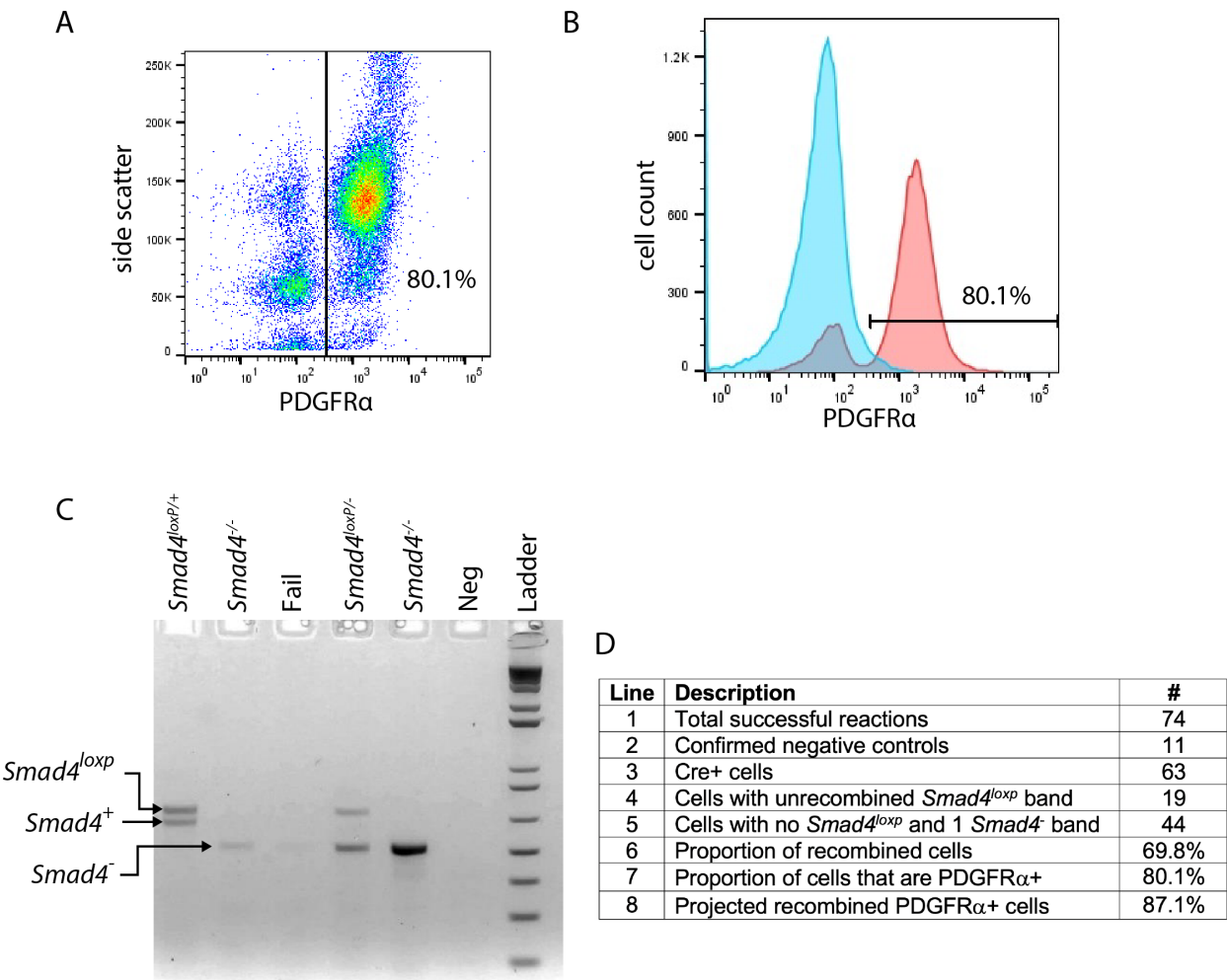


Fig. S1. *Smad4* is lost in renal interstitial cell precursors of *Smad4*^{IC} mice. (A) Flow cytometry showing percent PDGFRα⁺ in nephrogenic zone cells enriched by 3 rounds of magnetic selection. (B) Histogram comparing the enriched cell population stained with isotype control (blue) versus PDGFRα (pink); 80.1% of cells are PDGFRα⁺. (C) Gel electrophoresis of single cell genotyping PCR. Expected band sizes are 625bp for wild type (*Smad4*⁺), 675bp for non-recombined loxp (*Smad4*^{loxP}), and 512bp for null or recombined loxp (*Smad4*⁻) products. Amplification reactions resulting in ambiguous results (labeled “fail”) were not included in quantification. (D) Table of results for single cell genotyping: P0 kidneys from *Foxd1*^{+/-cre}; *Smad4*^{+/-} x *Smad4*^{loxP/loxP} were selected for GFP fluorescence (the *Foxd1* allele carries a GFP). Nephrogenic zone cells were enzymatically dissociated, PDGFRα - enriched and subjected to single cell genotyping. 81 cells were single cell amplified, of which 18 failed. 15 cells derived from wild type mice were included as contamination controls. 4 wild type negative

control cells failed. From a total of 74 successful reactions (line 1), 11 were negative controls that only showed amplification of the *Smad4*⁺ band (line 2), confirming that the assay is reliable. Of the remaining 63 cells (line 3), all tested positive for cre recombinase. Because one of the parents is *Smad4*^{loxp/loxp}, all offspring carry at least one *Smad4*^{loxp} allele that should be recombined by cre recombinase. Detection of a *Smad4*^{loxp} band (line 4) signifies either: a *Foxd1*-expressing cell in which cre-mediated recombination has not taken place, or that the cell is not a *Foxd1*-expressing cell (19.9% of the enriched cell population is PDGFRα-). Detection of a *Smad4*⁻ band with or without a *Smad4*⁺ band (line 5) signifies cells that have undergone cre-mediated recombination. The percentage of recombined cells (line 6), adjusted for the frequency of PDGFRα⁺ cells in the cell population (line 7) yields the predicted recombination frequency at the *Smad4* locus in *Foxd1*-expressing cells (line 8).

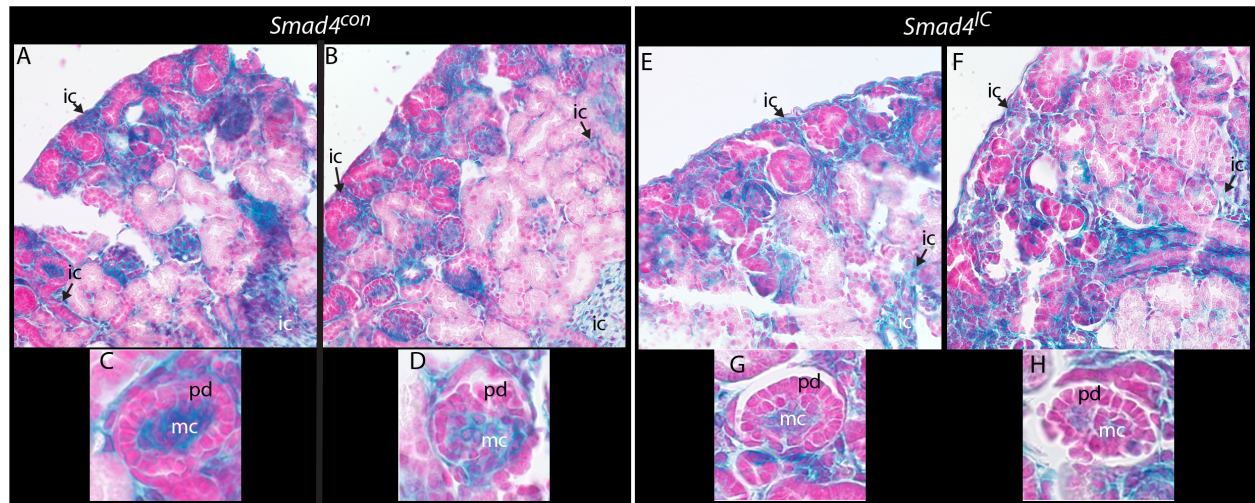


Fig. S2. Reporter gene expression reveals unchanged lineage commitment of *Foxd1*-derived cells in *Smad4*^{IC}. (A, B) X-Gal staining of kidney sections from 2 *Smad4*^{con} P0 pups on the R26R background. (C, D) High magnification images of glomeruli. (E, F) X-Gal staining of kidney sections from 2 *Smad4*^{IC} P0 pups on the R26R background. (G, H) High magnification images of glomeruli. Abbreviations: ic, interstitial cell; mc, mesangial cell; pd, podocyte.

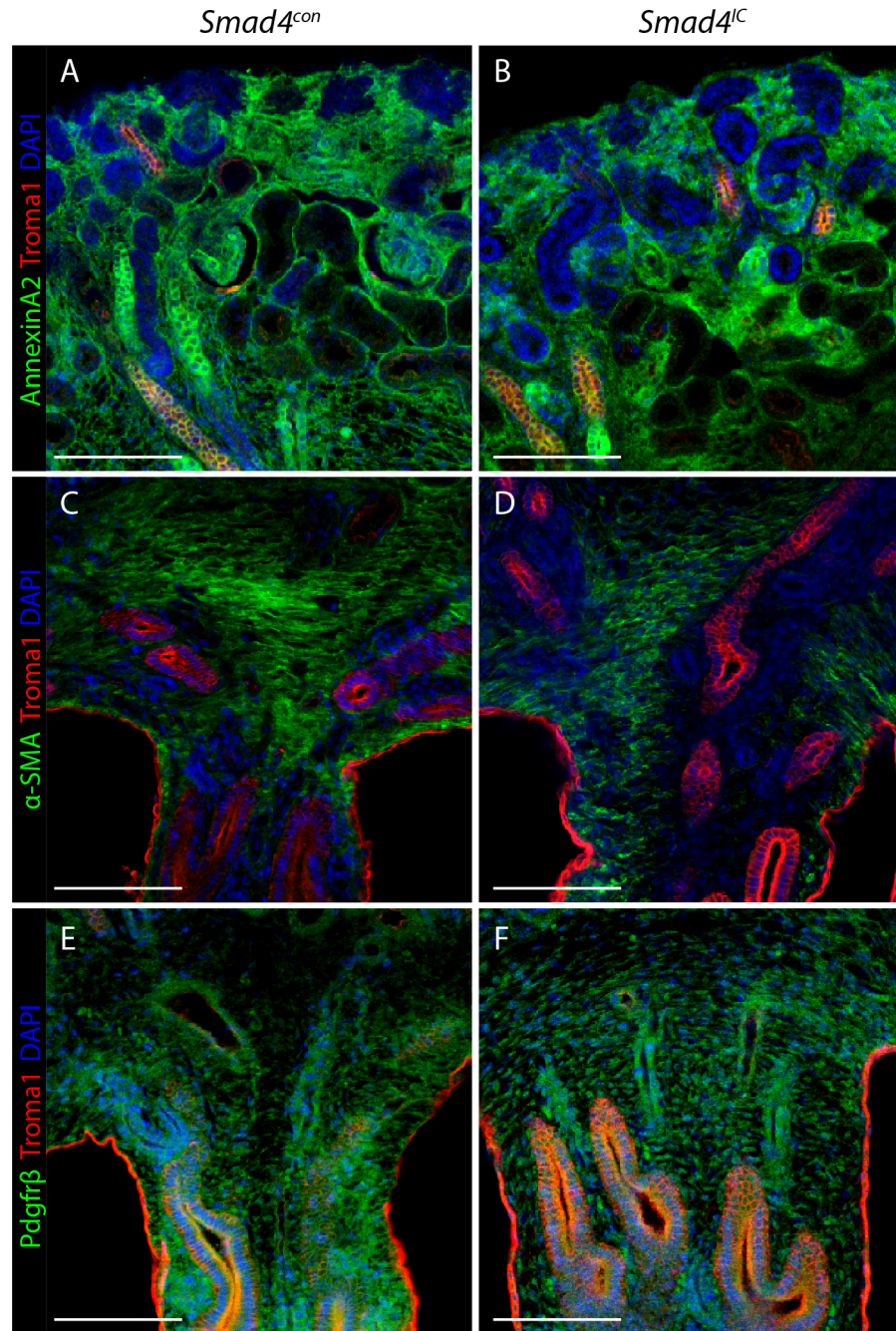


Fig. S3. No detectable phenotype is observed with loss of *Smad4* in the interstitium of E17.5 kidneys. Cortical (A, B) and medullary (C-F) regions of E17.5 kidneys immunostained for stromal marker AnnexinA2 (A, B; representative of n=6), α-SMA (C, D; representative of n=6) or PDGFRβ (E, F; representative of n=6) and counterstained with collecting duct marker TROMA-1 and DAPI. Scale bars: 200μm.

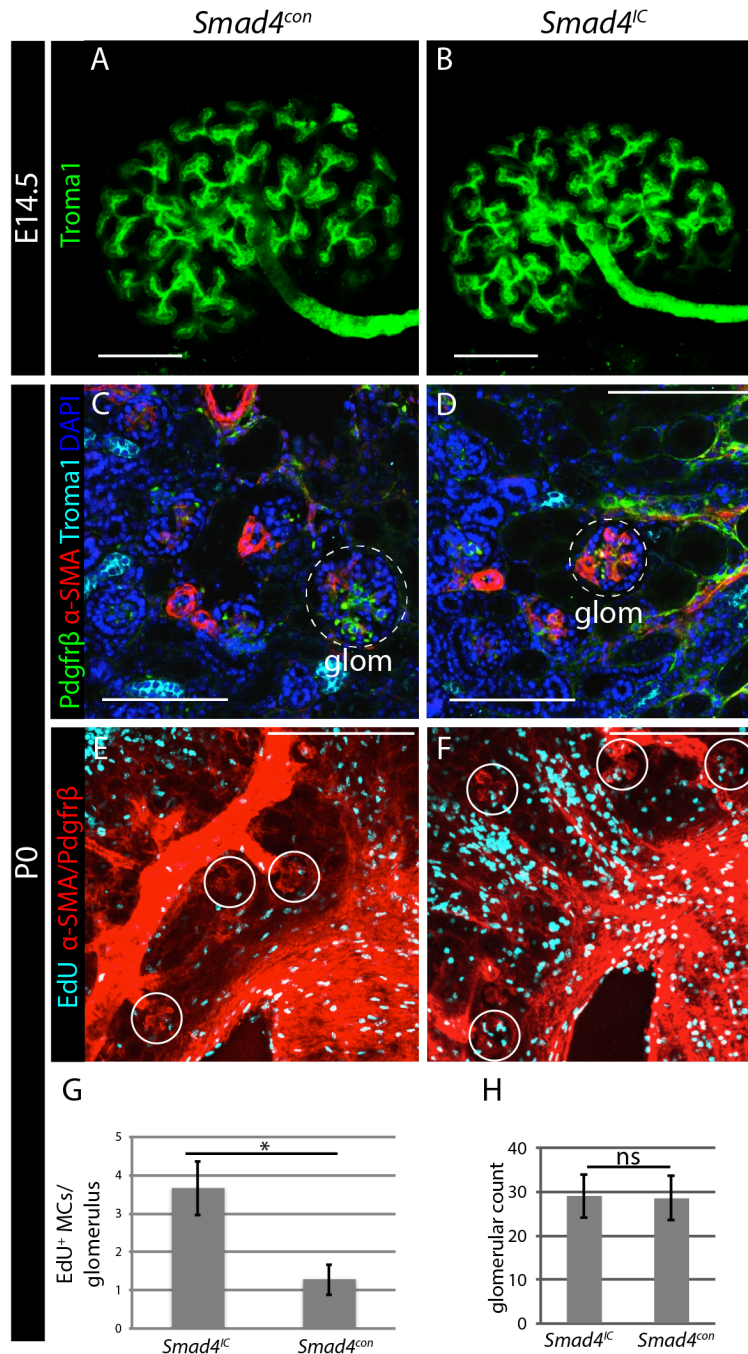


Fig. S4. Loss of *Smad4* does not affect early collecting duct branching but results in increased mesangial area and α -SMA expression and decreased mesangial proliferation. Representative confocal images of E14.5 kidneys from *Smad4*^{con} (A) and *Smad4*^{IC} (B) mice immunostained with TROMA-I that were used for 3D reconstruction (n=8). (C, D) Representative sections of P0 kidneys (n=8) costained with α -SMA, PDGFR β , TROMA-I and DAPI. Dashed circle denotes glomerulus (glom). (E, F) Representative epifluorescence images of kidney sections

from EdU-treated mice with glomeruli outlined. (G) EdU+/ α -SMA+ cells were quantified within each glomerulus in kidneys isolated from *Smad4^{con}* and *Smad4^{IC}* mice (n=6). (H) Number of glomeruli per field in *Smad4^{con}* and *Smad4^{IC}* kidneys at P0 (n=6). ns=p>0.05; *=p<0.05. Scale bars: 200 μ m in A, B.

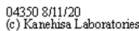
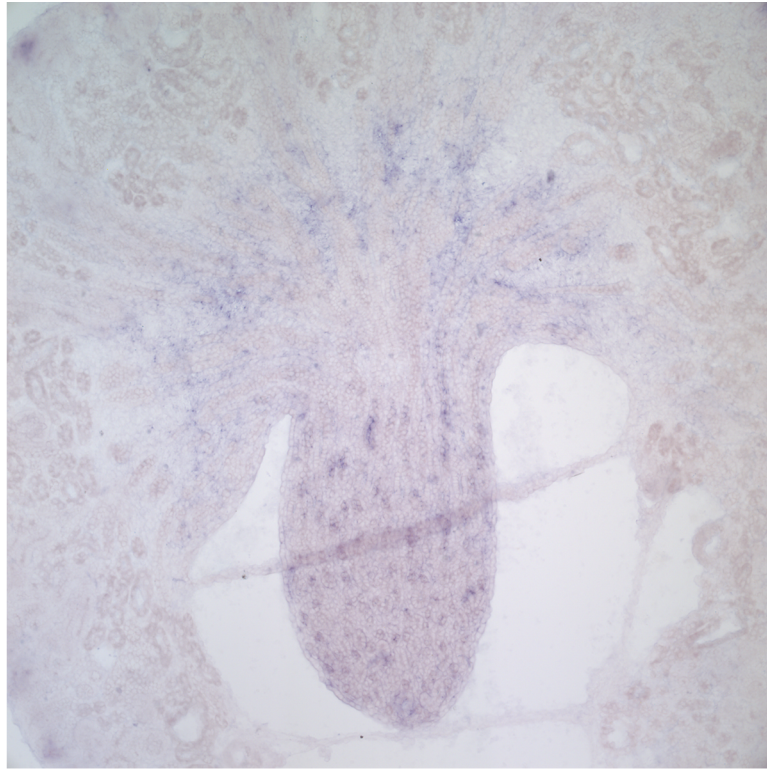


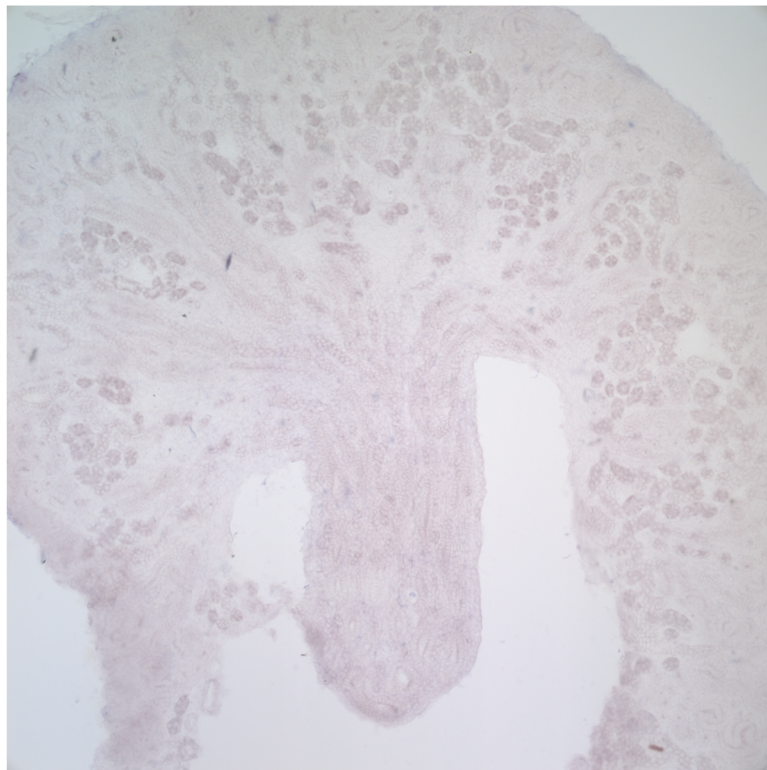
Fig. S5. TGF β pathway expression changes late in kidney development. (A) Kidney gene expression values were plotted for developmental time points E15.5, E16.5, E17.5, E18.5, and P0 neonates (N). Developmental time points are shown on the x axis and relative gene expression is shown on the y axis of each graph. (B) TGF β signaling schematic from KEGG showing pathway components down to the level of Smad4.

Smad4^{con}



Representative of
6 individuals

Smad4^{IC}



Representative of
4 individuals

Fig. S6. Axin 2 in situ hybridization. Representative sections showing signal localization in *Smad4*^{con} kidneys.

Table S1. Primary Antibodies used in this study.

target	company	clone	product number	application(s)
Troma1	DSHB	N/A	N/A	WM
PdgfrB	Abcam	Y92	Ab32570	WM, WB
a-SMA Cy3	Sigma	1A4	C6198	WM
a-SMA	Sigma	1A4	A2547	WB
Brn1				WM
Smad3	CST	C67H9	9523	TSA-WM
β -tubulin	SCB	H-235	sc-9104	WB
pSmad1/5/8	CST	N/A	9511	WB
Smad4	SCB	B-8	sc-7966	TSA-WM, WB
Lef1	CST	C12A5	2230	WM
p57kip2	CST	N/A	2557	WM
CyclinD1	CST	92G2	2978	WM
Ki67	Abcam	SP6	Ab16667	WM
AnnexinA2	CST	D11G2	8235	WM
pSmad1/5/8	V. Lindner	3131		TSA-WM

WB=western blot; WM=whole mount immunofluorescence; TSA-WM=Tyramide Signal Amplification whole mount immunofluorescence. Developmental Studies Hybridoma Bank (DSHB); Cell Signaling Technologies (CST); Santa Cruz Biotechnology (SCB).

Table S2. Nucleic acid sequences of primers used in this study.

mSmad4 W4	CTT TTA TTT TCA GAT TCA GGG GTT C
mSmad4 W2	AAA ATG GGA AAA CCA ACG AG
mSmad4 C2	TAC AAG TGC TAT GTC TTC AGC G
Cre 1	TTC GGC TAT ACG TAA CAG GG
Cre 2	TCG ATG CAA CGA GTG ATG AG
Hprt Cre Forward	GCT AAA GAG TTG AAC GCA AAG GTG
Hprt Cre Reverse	GGG CTA TGA ACT AAT GAC CCC GTA
Rosa26F2	AAA GTC GCT CTG AGT TGT TAT
Rosa1295	GCG AAG AGT TTG TCC TCA ACC
Rosa523	GGA GCG GGA GAA ATG GAT ATG